Measurements of Mixing Induced at a Gas Interface by the Richtmyer-Meshkov Instability

D. Ranjan, J. Niederhaus, J. Oakley,
M.H. Anderson, J. Greenough, R. Bonazza

July 2004

UWFDM-1298

Presented at the 24th International Symposium on Shock Waves (ISSW24), Beijing, China, 11-16 July 2004; published in *Shock Waves*, Z.L. Jiang (ed.), Paper 2691.

FUSION TECHNOLOGY INSTITUTE

UNIVERSITY OF WISCONSIN

MADISON WISCONSIN

Measurements of Mixing Induced at a Gas Interface by the Richtmyer-Meshkov Instability

D. Ranjan, J. Niederhaus, J. Oakley,
M.H. Anderson, J. Greenough, R. Bonazza

Fusion Technology Institute
University of Wisconsin
1500 Engineering Drive
Madison, WI 53706

http://fti.neep.wisc.edu

July 2004

UWFDM-1298

Presented at the 24th International Symposium on Shock Waves (ISSW24), Beijing, China, 11-16 July 2004; published in *Shock Waves*, Z.L. Jiang (ed.), Paper 2691.

Measurements of mixing induced at a gas interface by the Richtmyer-Meshkov instability

D. Ranjan[1], J. Niederhaus[1], J. Oakley[1], M.H. Anderson[1], J. Greenough[2], and R. Bonazza[1]

[1] *University of Wisconsin-Madison, Madison, WI, USA*
[2] *Lawrence Livermore National Laboratory, Livermore, CA, USA*

Abstract. Experiments to study the mixing between two gases induced by the Richtmyer-Meshkov instability are performed in a vertical shock tube of large, square internal cross section. The test gas is contained in an axisymmetric soap bubble which is at rest on an injector and is seeded with smoke to perform planar Mie scattering. Concurrently to the laboratory experiments, a computational investigation is carried out using the *Raptor* code– a finite volume code that solves the compressible Navier-Stokes equations using a Riemann solver with Phil Colella's Piecewise Linear Method for data reconstruction at cell interfaces. Differences between the computational and the laboratory experiments include: perfectly spherical *vs.* near-spherical, axisymmetric shape; diffuse interface with no soap film *vs.* soap interface with no diffusion; absence *vs.* presence of an injector to hold the bubble in place. Examples of experimental and computational images of shock-accelerated bubbles are shown below.

1 Introduction

The Richtmyer-Meshkov instability (RMI) results in the mixing of two gases of different density when the interface between them experiences an impulsive acceleration. This is an extension of the Rayleigh-Taylor instability (RTI), which is the evolution of the interface between two fluids of different densities subjected to a constant acceleration. Both instabilities originate from the baroclinic generation of vorticity at the interface due to the misalignment of the local pressure and density gradients; the vorticity production is constant over time in the RTI, while it is impulsive in the RMI. The RMI plays an important role in many areas of interest to scientists and engineers: improving supersonic mixing in a ramjet, supernova expansion [1], and inertial confinement fusion where dilution of the fuel lowers fusion yield [2].

Experimentally, the RMI presents many challenges, the greatest of which is preparation of the initial interface. Meshkov [3] was the first experimenter to study a shock wave-accelerated gas-gas interface; he used a thin nitrocellulose film to separate the test gases, a technique that has been commonly used in many subsequent experiments. However, there are several well-documented problems with using films: first, the strength of the film and supporting wires can weaken the transmitted shock wave; second, post-shock fragments of the film and wires affect the fluid flow; and third, these same fragments hinder diagnostic and imaging techniques.

For these reasons, different preparation methods have been developed to eliminate the film and have a continuous interface. Brouillette and Sturtevant [4] and Bonazza and Sturtevant [5] used a thin flat sliding plate in a vertical shock tube to initially separate the two gases in a light over heavy configuration. The physics of the plate retraction create the initial condition in the vertically stratified gases. The initial conditions in this case can be non-linear and multi-valued due to vortex shedding off of the plate.

Also, run to run repeatability is not particularly good. Jacobs *et al.* [6] used a gas curtain to create two continuous interfaces. Jones and Jacobs [7] used a flow technique to create a flat interface, and then oscillated their vertical shock tube side-to-side to create the initial perturbation. Due to the long contact time between gases in these methods, the interface is diffuse in nature with a relatively large diffusion thickness. Oakley [8] used a sinusoidally formed plate to separate the two gases (initially arranged in the gravitationally unstable configuration) and allow the Rayleigh-Taylor instability to create the initial perturbation. In a cross-sectional view perpendicular to the direction of plate retraction, the initial condition looks two-dimensional; however, due to disturbances in the direction of plate retraction, the interface has three-dimensional characteristics.

In the present experiments, the interface between the two different gases consists of soap film (specifically a mixture of water, liquid soap and glycerin). A soap film is more acceptable than a mylar or nitrocellulose membrane to set up an interface in that, upon shock acceleration, the bubble breaks up into much smaller fragments (droplets) than the membrane; hence the effects on the fluid flow and its observability are much smaller than the membrane's. A soap bubble has been used in the past [9] to prepare an interface to be subjected to shock acceleration; the long term objective of the present program is to improve upon the initial configuration (releasing the bubble into free fall or free rise) and the diagnostic techniques (from Schlieren to planar, quantitative imaging).

2 Experiment Description

The experiments are performed in the Wisconsin Shock Tube Facility [10]. The tube is vertical, with square internal cross section, 25×25 cm; its length is 9.2 m, with a 1.8 m long driver section, located at the top of the tube. A downward-moving shock wave is released by discharging a boost tank, through a fast-opening valve, into the driver section, prepressurized to about 95% of diaphragm rupture pressure; with this technique, control of shock release time is within ±5 ms. In all the present experiments the driven is either N_2 or Ar and the bubble is Ar or N_2, respectively; the shock Mach number is 2.13 (N_2) or 2.01 (Ar), corresponding to a shock speed of 752 m/s (N_2) or 649 m/s (Ar) in the driven gas and a post-shock bubble velocity of 489 m/s (N_2) or 366 m/s (Ar). For early time shock-bubble interaction studies the bubble is prepared and imaged in the test section, located 6.545 m below the diaphragm, and for late time studies it is prepared in the interface section located 6.095 m below the diaphragm and imaged in the test section. Planar Mie scattering is performed by loading the bubble test gas with smoke (at 0.5% mass fraction) and shining a laser sheet (at 532 nm) from a Continuum SLIIPIV Nd:YAG through the midplane of the shock tube cross section. The images are captured with an Andor DV434-BU2 CCD camera. The outputs from several piezoelectric transducers mounted at various distances along the tube are used to trigger the laser and data acquisition electronics. Figure 1 shows a schematic of the experimental setup.

3 Numerical Simulation

The adaptive mesh refinement (AMR) hydrodynamics code *Raptor*, utilizing monotonicity preserving methods [11], is used for the computer simulations of a spherical bubble. The spherical bubble is studied in a two-dimensional domain using r-z symmetry. The

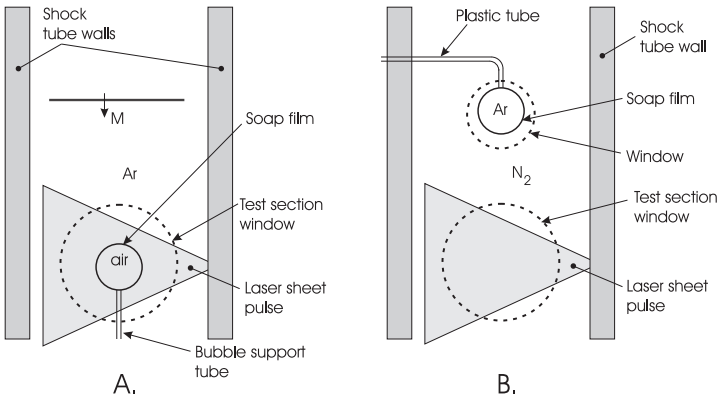

Fig. 1. Schematic of vertical shock tube test section. (A) For early time shock-bubble interaction studies a light bubble (air) is prepared in the test section filled with Ar. The laser beam is timed to pulse when the shock interacts with the bubble. (B) For later time experiments, a heavy (Ar) bubble is prepared 45 cm above the center of the test section which is filled with air. The camera line of sight is centered at the window and is perpendicular to the laser sheet.

cylindrical domain has a radius of 12.5 cm and a length of 75 cm. Shocked driven gas properties fill the top 1 cm of the domain allowing the shock to propagate down the length of the domain into the bubble (8.5 cm diameter, centered at r=0 and 10 cm from the top of the domain). The interface between the bubble and driven gases is modeled as a diffuse 1.5 mm layer while accounting for the presence of the soap film will be a focus of future investigations. The domain is comprised of square mesh elements (50×300) and utilizes three levels of AMR at ratios of 4, 4 and 2 resulting in a spatial resolution of 0.08 mm. A symmetry boundary condition is used at r=0, while outflow is used at the remaining three boundaries. Richardson extrapolation is used to ensure shock waves are refined and a Sutherland model is used for molecular viscosity.

4 Results

In a first set of laboratory experiments, the driver gas is nitrogen, the driven gas is argon and a soap bubble filled with air (test gas) sits on an injector inside the test section, facing upwards because of buoyancy; an M=2.13 shock wave impacts the bubble from above. The air is seeded with smoke (at about 0.5% mass loading). computational experiments, the soap film is not modeled; the interface is 2 show the bubble (diameter≈6.5 cm) at the earliest post-shock times: initially, the only effect of the shock traversal of the bubble is to compress the air inside it, with no visible mixing occurring with the surrounding argon. Since the initial bubble size inevitably varies from run to run, comparison between the laboratory and the computational experiments is performed using data from the times when the shock has traversed approximately the same fraction of the bubble diameter, as shown in Fig. 3. Agreement of the geometrical parameters is excellent; no experimental measurement of the shocked air density is available but, since no mixing with the surrounding argon has yet taken place, there is no reason to suspect that the density should differ from the value that can be calculated using shock-refraction physics.

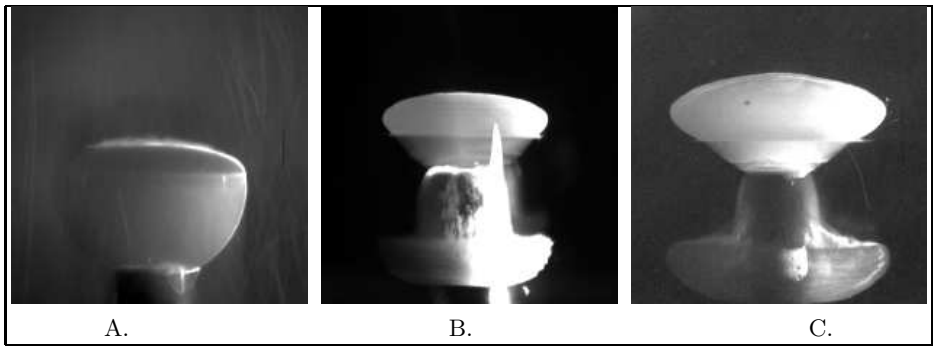

Fig. 2. Experimental images for a M=2.13 shock in Ar incident on a bubble of air seeded with smoke particles, times are given from when the shock is at the top of the bubble. (A) $t \approx 33$ μs, (B) $t \approx 61$ μs, and a portion of the image is washed out due to saturation of the CCD, (C) there are two pulses from the laser, the first is at $t \approx 66$ μs and the second, at a much later time is at $t \approx 191$ μs.

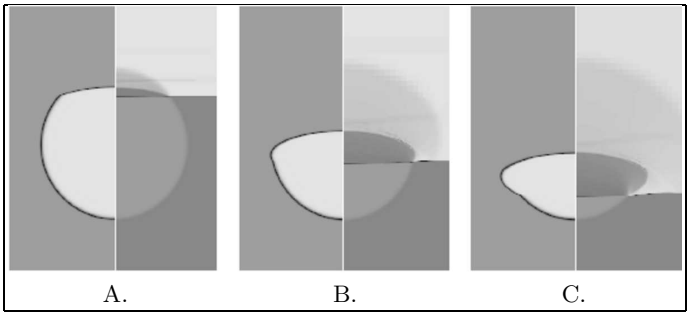

Fig. 3. Computational images for a M=2.13 shock in Ar incident on a bubble of air, times are given from when the shock is at the top of the bubble. The left half of each image is mass fraction and the right half is density. (A) $t \approx 20$ μs, (B) $t \approx 73$ μs, and (C) $t \approx 100$ μs.

At later post-shock times, the bubble distorts and ruptures, its shape departs dramatically from simple compression, and mixing of the two gases becomes very significant; but the injector used to support the bubble in the first experimental series would both obstruct the view of the bubble and grossly affect the flow. Thus a different initial geometry is used, with the bubble hanging from an L-shaped injector, facing downwards, as shown in Fig. 1B. In this configuration, buoyancy would have the adverse effect of pushing the bubble upwards, into the side of the injector, thus this time the bubble contains the heavy gas (argon) seeded with smoke (0.5% mass fraction and also approximately 20% mass fraction N_2); the driver and driven gas are N_2 and the shock strength is M=2.01. As seen in Fig. 4, because of gravity and of the accumulation of some bubble solution towards the bottom of the bubble, its shape is not spherical but is still very close to axisymmetric; in the experiments, the length of the vertical bubble axis ranged Δy=5.4–5.5 cm, while that of the horizontal axis ranged Δx=4.7-5.4 cm. The images in Fig. 5 show the qualitative run to run repeatability in the overall bubble distortion and rupture patterns. The bubbles with more sag, Figs. 5A and C, show a smaller additional vortex

ring (appearing in this planar image as a vortex pair) above the main vortex ring while this feature is largely suppressed in the case of a more symmetrical initial condition, Fig. 5B. The vortex ring that develops above the bubble is due to the modal nature of the curvature at the top of the bubble and this has been witnessed previously in a study of a copper sphere subjected to a M=10 shock wave [12]. Figure 6 shows the results of a computational run for a spherical bubble. The computational run shows less diffuse mixing in the main vortex ring than the experiment, and it does predict the presence of the smaller upper vortex ring.

Fig. 4. Initial condition for hanging bubble filled with Ar. The shape deviates from a sphere due to sag from both the Ar being heavier than the N_2 driven gas and also the small accumulation of bubble fluid visible at the bottom of the bubble.

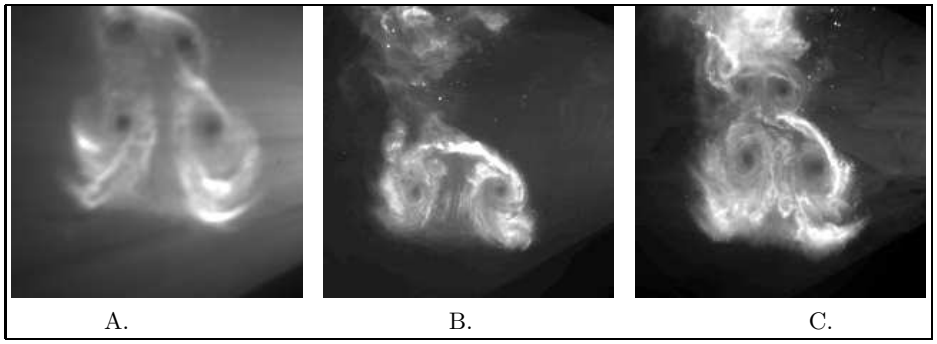

Fig. 5. Experimental images for a M=2.01 shock in N_2 incident on a bubble of Ar seeded with smoke particles, times are given relative to the time when the shock is at the top of the bubble. (A) $t \approx 1.15$ ms, Δy=5.4 cm, Δx=4.7 cm, (B) $t \approx 1.18$ ms, Δy=5.5 cm, Δx=5.4 cm, (C) $t \approx 1.18$ ms, Δy=5.5 cm, Δx=4.8 cm.

5 Conclusions

The preliminary results discussed here show that a soap bubble is a suitable means to prepare an interface for shock acceleration. The observed shape distortion and rupture and the mixing between different gas species that follows represent an ideal testbench for hydrodynamic codes like *Raptor*. The next two goals of the present program are to

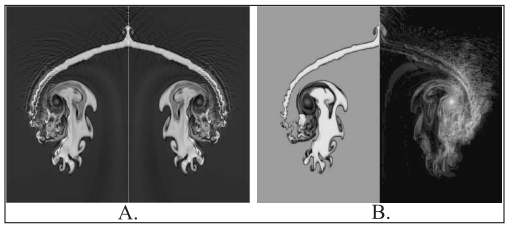

Fig. 6. Computational images for a M=2.01 shock in N_2 incident on a bubble of Ar at $t \approx 1.18$ ms. (A) Density plot, left is mirrored for visualiztion comparison to experimental images, (B) left side is mass fraction and the right side highlights the locations of strong negative vorticity.

release the bubble from the injector (so that it moves freely upwards or downwards inside the shock tube at the time of shock acceleration) and to complete the implementation of planar laser induced fluorescence to quantify the mixing phenomena.

6 Acknowledgements

The authors would like to acknowledge the financial support of the Department of Energy (through grant No. DE-FG03-98DP00207).

References

1. B. Jun, T. W. Jones, M. L. Norman: "Interaction of Rayleigh-Taylor fingers and circumstellar cloudlets in young supernova remnants", The Astrophysical Jounal **468**, (1996) L59-L63
2. J. D. Kilkenny: "A review of the ablative stabilization of the Rayleigh-Taylor instability in regimes relevant to inertial confinement fusion", Phys. Plasmas **1**, 5 (1994) pp. 1379–1389
3. Ye. Ye. Meshkov: "Instability of a shock wave accelerated interface between two gases", NASA Technical Translation F-13,074 (1970)
4. M. Brouillette, B. Sturtevant: "Experiments on the Richtmyer-Meshkov instability: small scale perturbations on a continuous interface", Phys. Fluids **5** 4 (1993) pp. 916–930
5. R. Bonazza, B. Sturtevant: "X-ray measurements of growth rates at a gas interface accelerated by shock waves", Phys. Fluids **8** 9 (1996) pp. 2496–2512
6. J.W. Jacobs, D.G. Jenkins, D.L. Klein, R.F. Benjamin: "Instability growth patterns of a shock-accelerated thin fluid layer", Phys .Rev. Lett **70** 5 (1993) pp. 583–586
7. M.A. Jones, J.W. Jacobs: "A membraneless experiment for the study of Richtmyer-Meshkov instability of a shock-accelerated gas interface", Phys. Fluids **9** 10 (1997) pp. 3078–3085
8. J.G. Oakley: Experimental Study of Shocked Gas Interfaces with Visualized Initial Conditions. PhD Thesis, University of Wisconsin-Madison, WI (2001)
9. J.H Haas and B. Sturtevant: "Interaction of weak shock waves with cylindrical and spherical gas inhomogeinities", JFM **181** (1987) pp. 41–76
10. M.H. Anderson, B.P. Puranik, J.G. Oakley, P.W. Brooks, R. Bonazza: "Shock tube investigation of hydrodynamic issues related to inertial confinement fusion", Shock Waves **10** (2000) pp. 377–387
11. W. Rider, J. Greenough, J. Kamm: 'Extrema, accuracy and monotonicity preserving methods for compressible flows'. *16th AIAA Fluid Dynamics Conference*, AIAA Paper 2003-4121 (2003)
12. R.I. Klein, K.S. Budil, T.S. Perry, D.R. Bach: "The interaction of supernova remnants with interstellar clouds: experiments on the NOVA laser", The Astrophysical Journal **583** (2003) pp. 245–259